Photosensitized Silica Nanoparticles

Subjects: Chemistry, Physical
Contributor: VIRGINIA MARTINEZ

BODIPY dyes have recently attracted attention as potential photosensitizers. Commercial and novel photosensitizers (PSs) based on BODIPY chromophores (haloBODIPYs and orthogonal dimers strategically designed with intense bands in the blue, green or red region of the visible spectra and high singlet oxygen production) were covalently linked to mesoporous silica nanoparticles (MSNs) further functionalized with PEG and folic acid (FA).

Keywords: BODIPY-based photosensitizers ; functionalized silica nanoparticles ; folic acid ; PEG ; photodynamic therapy

1. Introduction

Currently, several alternatives are used to treat cancer, including surgery and chemo, radio- or immune-therapy, although depending on the type of cancer an effective method has not been found yet. In this regard, Photodynamic Therapy (PDT) is a complementary treatment that can be applied as a combined therapy to enhance anticancer efficiency by a synergic or additive effect with conventional methods. PDT involves a light source, a photosensitizer (PS), and oxygen. During PDT, PS is activated under light at a specific wavelength to generate reactive oxygen species (ROS), mainly singlet oxygen ($^1O_2$), a cytotoxic species able to promote apoptosis or necrosis of cancer cells [1]. Nowadays, preclinical and clinical trials have proven PDT to be effective in early-stage tumors or the palliation of advanced cancers, such as skin, head, neck, esophageal, or lung cancer, improving patient survival [2][3][4][5]. PDT is considered a less invasive and more precise treatment (locally controlled by the light irradiation of malignant tissue), without inducing long-term side effects, and it has a lower cost with respect to other treatments. Nevertheless, the limitations of PDT are mainly related to the availability of the PSs. Despite there being several PSs approved by the FDA, most of them are hydrophobic and/or tend to have poor selectivity to malignant tissues [6][7][8][9].

The ideal PS to be used as a photoactive drug for PDT should be non-cytotoxic in dark conditions, selective to cancer tissues, and display limited stability in vivo to minimize side effects; it should have intense absorption bands ($\varepsilon \geq 50{,}000$ M^{-1} cm^{-1}), preferentially in the phototherapeutic window to ensure deeper penetration of light into tissues [10] (630–850 nm), and high singlet oxygen production to reduce doses and irradiation time; it should be photoresistant to avoid the photodecomposition of the PS during treatment; and finally, it should present an amphiphilic nature, being soluble in water as well as permeable through the cell membrane. At the moment, few PSs fulfill these requirements, and new molecular designs are required [6][7][11][12][13][14]. One approach for obtaining new molecules is focused on the synthesis of improved PS to overcome their limitations, but this usually requires multistep chemistry, increasing the costs and production time, hampering the implementation for clinical uses. In this context, BODIPY dyes have recently attracted attention as potential photosensitizers [15][16][17][18]. They are characterized by intense absorption and emission bands in the green region, and resistance to photobleaching [19][20]. Despite being highly fluorescent chromophores (antagonistic property to ROS generation) and poorly soluble in water, their synthesis allows easy, versatile, and selective modification of their molecular structure to increase the population of the triplet state, and consequently their singlet oxygen generation, while also shifting their spectroscopic bands into the clinical window. These modifications include the addition of iodine heavy atoms, π-conjugated systems in the BODIPY skeleton, or the design of orthogonal BODIPY dimers [15][17][18][21][22][23][24][25][26][27][28][29][30][31][32][33]. Further functionalization of the BODIPY chromophore is related with the incorporations of different targets to increase their solubility in aqueous media and enhance their selectivity to cancer cells [14][34][35][36][37][38][39].

Another alternative is the use of nanomaterials as (photo)drug carriers. They have a large surface-to-volume ratio, which allows the administration of a large amount of active components, preventing their degradation or inactivation by plasma components, delivering soluble and stable formulations in aqueous media, and enhancing their accumulation inside tumor tissues by so-called passive targeting due to the enhanced permeability and retention (EPR) effect [11][40][41][42][43][44][45][46][47][48][49]. Additionally, the selectivity to cancer cells can be improved by active targeting through surface modifications with target ligands, such as proteins, polysaccharides, nucleic acids, peptides and small molecules that bind to specific receptors overexpressed on the surface of malignant cells but not on healthy cells [9][50][51][52].

Currently, there are many different types of nanoparticles based on liposomes, polymeric, micellar, metallic, or protein for medical use [40][41][42][43][44][45][46][53][54][55]. In this regard, silica nanoparticles (SN) have attracted attention as carriers for drug delivery due to their properties, which include reduced toxicity, good biocompatibility, high surface area, easy functionalization, optical transparency, and low cost [56][57]. PS-loaded silica nanoparticles have been reported as promising singlet oxygen generator platforms, improving the photoactive drug delivery by enhancing PS poor solubility and selectivity for cancer cells [58][59][60][61][62]. The PS can be physically encapsulated or covalently attached to the internal or external surface of the silica nanoparticles [63][64][65][66][67]. Briefly, loading PS within the nanostructure ensures a high photostability but restrains the diffusion of oxygen species (molecular oxygen towards inside and singlet oxygen towards outside). It has been demonstrated that nanoparticles with draped-PS outside lead to better $^1O_2$ productivity than PS located inside [68][69][70].

In the last few years, diverse nanoplatform designs have been used as vehicles to carry BODIPY-PS [71][72][73][74][75][76][77][78][79][80][81], or even BODIPY-based nanoparticles, through the self-assembly process [79][80][82][83][84][85][86][87][88]. However, despite the advantageous properties of SN, mentioned above, few examples can be found in the literature of their use as carriers for BODIPY-PSs [89][90].

In this work, different PSs (**Figure 1**) were tethered to the external surface of 50 nm MSNs. First, three commercially available PSs, Rose Bengal (RB), Chlorin e6 (C6), and Thionine (Th), recognized as suitable singlet oxygen generators and extensively employed in PDT, were used [6][9][10][11][59][91][92][93]. These dyes already have functional groups in their molecular structure (carboxylic in Rose Bengal and Chlorin e6 and amine in Thionine) and can be easily grafted to the external surface of MSNs. Afterward, seven custom-made BODIPY-based PSs were used, which were rationally designed to effectively generate high singlet oxygen production under illumination at different wavelengths of the visible spectra (blue, green or red light) [12][18][24][31][94][95], and to endow suitable graftable groups to be anchored at MSNs.

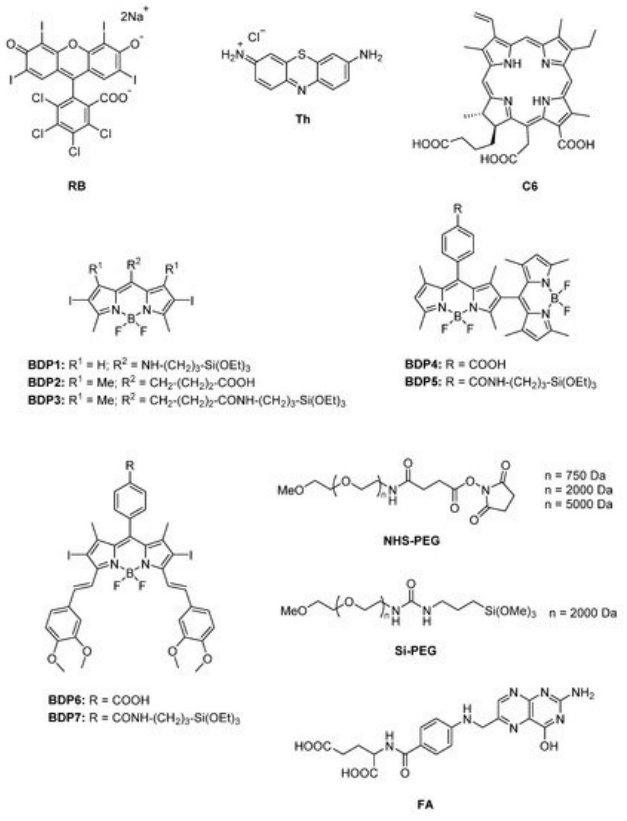

Figure 1. Molecular structure of the different compounds anchored to MSN: commercial (RB, Th, C6) and custom-made BODIPY photosensitizers (BDP1-BDP7), PEG derivatives with different functional groups (Si-PEG and NHS-PEG) and molecular weight (750 Da, 2000 Da and 5000 Da), and FA.

Additionally, MSNs were externally coated with polyethylene glycol (PEG), as it is usually required to stabilize nanoparticle systems, enhance their life-time in the blood system and avoid the induction of immune responses [44][47][49][94][95][96][97][98]. For that, several PEG derivatives (**Figure 1**) with different graftable groups at one end of the chain (succinimide group or with silyl group Si-PEG) were tethered at the MSN shell. The length of the polymer chain (750 Da, 2000 Da, and 5000 Da) was also adjusted to improve nanoparticle stabilization in water.

2. Silica Nanoparticles Characterization

Mesoporous silica nanoparticles with a suitable size for medical applications and particularly for PDT [98][99] were synthesized by the modified Stöber method [100] as described elsewhere [101]. The external surface of mesoporous nanoparticles surface was functionalized with amino group (NH-MSN) or carboxylic group (COOH-MSN). The latter type was obtained after conversion of CN-MSN in acidic conditions, according to the synthesis route described in Materials and methods section and Supporting Material. Bare MSNs analyzed by SEM and TEM showed spherical morphology and mesoporous structure (**Figure 2**), with a size distribution of 50 ± 10 nm. The external functionalization of MSNs was studied by XPS. The presence of 5% of nitrogen atoms in both NH-MSN and CN-MSN confirmed the existence of amine/cyano functional groups located outside of the nanoparticles whereas the absence of nitrogen atoms in the COOH-MSN indicates an effective conversion of CN into COOH groups. In the case of FTIR spectra, an intense peak located at υ = 1110–1000 cm^{-1} as well as a wide band placed at υ = 3650–3200 cm^{-1} were recorded in every sample spectrum, and are assigned to Si-O-C and O-H groups, respectively. A characteristic band of cyane group (C≡N) at υ = 2260–2240 cm^{-1} was recorded in CN-MSN, which disappeared in the COOH-MSN system, indicating again the total conversion from -CN to -COOH. Furthermore, the typical band of COOH group (COO-H υ = 3550–2550 cm^{-1}, C=O υ = 1775–1650 cm^{-1}) was also registered in COOH-MSN.

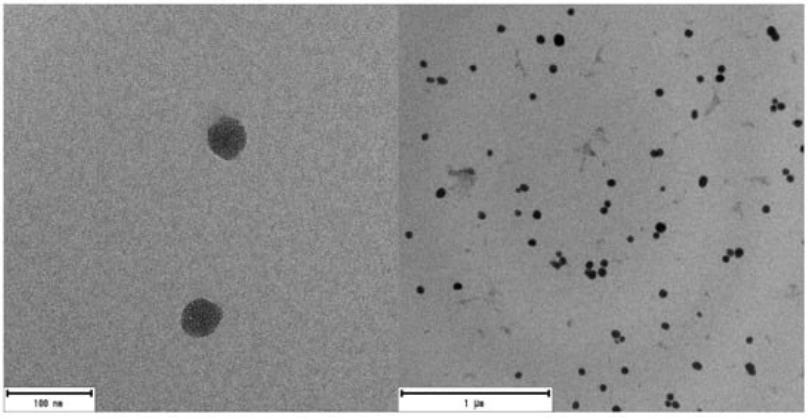

Figure 2. TEM images of MSNs. There are no noticeable differences between any of the synthesized MSNs (NH-MSN, CN-MSN and COOH-MSN).

The sizes of the three types of nanosystems were also characterized in water suspension by DLS. Both NH-MSN and COOH-MSN showed similar hydrodynamic diameter, of around 60–70 nm, to the size of the nanoparticles by TEM (**Table 1**), whereas the larger diameter, derived for CN-MSN, of 280 nm, indicates a tendency to form aggregates. Zeta potential values obtained for CN-MSN but also for NH-MSN (≤±25 mv) [102] confirm a poorer stability in water with respect to COOH-MSN system. The higher stability of this later functionalized COOH-MSN is attributed to the presence of carboxylic groups at the external surface, partially deprotonated (COO^-) in aqueous media and the superficial negative charge makes the nanosystem more stable by electrostatic repulsion, **Table 1**.

Table 1. DLS and Zeta potential of mesoporous silica nanoparticles in water.

Name	Shell	DLS (nm)	Z Pot (mV)
NH-MSN	**NH_2/OH**	**71**	**−3.96**
CN-MSN	**CN/OH**	**280**	**−7.06**
COOH-MSN	**COOH/OH**	**66**	**−39.7**

Actually, the MSNs' stability in aqueous media is certainly controlled by the type and the number of molecules lodged at the external surface. It has been demonstrated that the presence of organic PSs makes the external surface of MNS more hydrophobic, promoting nanoparticles agglomeration, hindering their stability in aqueous media [103]. Note here that the particle–particle aggregation is detrimental to singlet oxygen production and should be avoided or minimized. To optimize the PS loading and to ensure the stability of the nanoparticles in suspension, several syntheses were carried out for the amine-functionalized MSN (NH-MSN), employing commercial RB as PS and different PEG derivatives (RB-PEG_n-NH-MSN). The combinations were focused on the variation of (i) the functional group of the MSN (OH-, or NH_2-) at which PS and PEG molecules were attached, and (ii) the length of PEG chain (750 Da, 2000 Da, and 5000 Da).

3. Optimization of the Functionalization of Silica Nanoparticles with Rose Bengal as PS

Rose Bengal is a commercial PS with an intense absorption band (λ_{max} = 556 nm; ε = 9.8·10^4 M^{-1}cm^{-1}) and high singlet oxygen production (Φ_Δ = 0.86 in CH_3OD). The carboxylic function in the RB molecular structure allows the covalent grafting to be inserted to amine groups or to the intrinsic hydroxyl groups of the external surface of MSN [103]. Nevertheless, both RB-MSN nanosystems (RB grafted at the external NH_2 or OH) showed instantaneous flocculation in water media and the suspension was only viable in less polar solvents. Since stable nanoparticle suspension in water is crucial to obtain competitive hybrid nanocarriers for PDT [103], pegylation of the outside of MSNs is required to avoid the precipitation of the nanoparticles. Firstly, to optimize the stabilization of the system, NHS-PEG of different chain length (750 Da, 2000 Da and 5000 Da) were linked to the amine groups of the silica, while RB was anchored in OH groups (samples RB-PEG$_{750}$-NP-**a**, RB-PEG$_{2000}$-NP-**a**, and RB-PEG$_{5000}$-NP-**a** in **Table 2**).

Table 2. RB amount, nanoparticle size and their Zeta potential by DLS in water of the different RB-PEG-MSNs.

System	Characteristic	PEG Length (Da)	DLS Size (nm)	ZPOT (mV)	[RB] (μmol/g)
RB-PEG$_{750}$-NP-a	**RB-OH-MSN PEG-NH$_2$-MSN**	**750**	**130**	**−4.3**	**20**
RB-PEG$_{2000}$-NP-a	**RB-OH-MSN PEG-NH$_2$-MSN**	**2000**	**99**	**−25.0**	**20**
RB-PEG$_{5000}$-NP-a	**RB-OH-MSN PEG-NH$_2$-MSN**	**5000**	**114**	**−25.0**	**20**
RB-PEG-NP-b	**RB-NH$_2$-MSN PEG-OH-MSN**	**2000**	**95**	**−29.0**	**10**
RB-PEG-NP-c	**RB-OH-MSN PEG-OH-MSN**	**2000**	**88**	**−31.0**	**20**

According to zeta potential (**Table 2**), the least favored value (−4.3 mV) was registered for sample RB-PEG750-NP-a with the shortest PEG chain in this series, indicating its inefficiency at improving the stability of RB-MSN in water. Indeed, a similar value of around -4 mV was obtained for NH-MSN without RB (**Table 1**). In contrast, PEG of higher molecular weight, 2000 Da and 5000 Da (RB-PEG$_{2000}$-NP-**a** and RB-PEG$_{5000}$-NP-**a** in **Table 2**) rendered Zpot values of −25 mV, indicating good stability of these nanosystems in water. The longer PEG-5000 did not lead to an improvement of the stability with respect to PEG-2000, which could likely be assigned to a different conformation adopted at the external surface [104]. Additionally, long PEG chains can also impede the internalization of nanoparticles into the cells [105][106]. Thus, a PEG of 2000 Da was selected as the most suitable, and was employed in the rest of the samples.

Next, different anchorages between PEG and MSN (at a fixed PEG length of 2000 Da) were also tested. The anchoring of Si-PEG (silylated PEG of 2000 Da, **Figure 1**) to the external OH-groups of MSN, samples RB-NP-**b** and RB-NP-**c**, led to even higher Zpot values with respect to sample RB-PEG$_{2000}$-NP-**a** (with PEG at the amine groups), **Table 2**. This fact is possibly due to a higher presence of PEG at the surface because there are more accessible OH-groups than NH_2-groups at the silica external surface [97]. This assumption was confirmed for RB, showing a double dye loading when was tethered to OH with respect to NH_2 groups of the MSN external surface (RB-PEG-NP-b vs. RB-PEG-NP-**c** in **Table 2**) [103].

The stability of the nanoparticles can also be studied by the absorption spectra of the RB-PEG-MSNs samples in water suspension (**Figure 3**). The registered bands for RB-PEG$_{2000}$-**a** and RB-PEG$_{5000}$-**a**, practically identical, showed more prominent shoulders at both sides of the main absorption band, indicative of a higher dye aggregation tendency. Indeed, according to the absorption spectra, the dye aggregation follows the tendency RB-PEG$_{5000}$-NP-**a** ≈ RB-PEG$_{2000}$-NP-**a** > RB-PEG-NP-**c** > RB-PEG-NP-**b**. For the samples RB-PEG$_{2000}$-NP-**a**, RB-PEG$_{5000}$-NP-**a**, and RB-PEG-NP-**c** (RB grafted at the hydroxyl groups of MSNs, **Table 2**) the estimated RB loading was equal, and consequently, the observed dye aggregation in these samples should be assigned to interparticle processes, as supported by Zpot values and previously attributed to a lower presence of PEG molecules at the external surface. Sample RB-PEG-NP-**b**, with RB loading at the amine groups half of that obtained for the RB at the hydroxyl groups (sample RB-PEG-NP-**b** vs. sample RB-PEG-NP-**a** in **Table 2**), showed a narrower absorption band, not much different from that recorded for RB in diluted solution [101]. However, reducing the cargo of PS per nanoparticle would compel a higher concentration of nanoparticles per volume to reach effective PS doses for PDT in the cells, which would also promote particle-particle agglomeration. For this reason, the optimization of the samples is not a trivial task, and the quantification of their singlet oxygen production would be a good indicator of their applicability in cells. Significantly, all the samples, except for RB-PEG$_{750}$-NP-**a**, showed a similar

singlet oxygen quantum yield, with values around $\Phi_\Delta \approx 0.80–0.85$ in deuterated methanol (CH_3OD), similar to that registered for RB in the same solvent ($\Phi_\Delta = 0.86$). The fact that RB grafted to MSN can generate singlet oxygen as efficiently as the RB in solution is indicative of the potential use of these nanosystems in PDT [65][67][102].

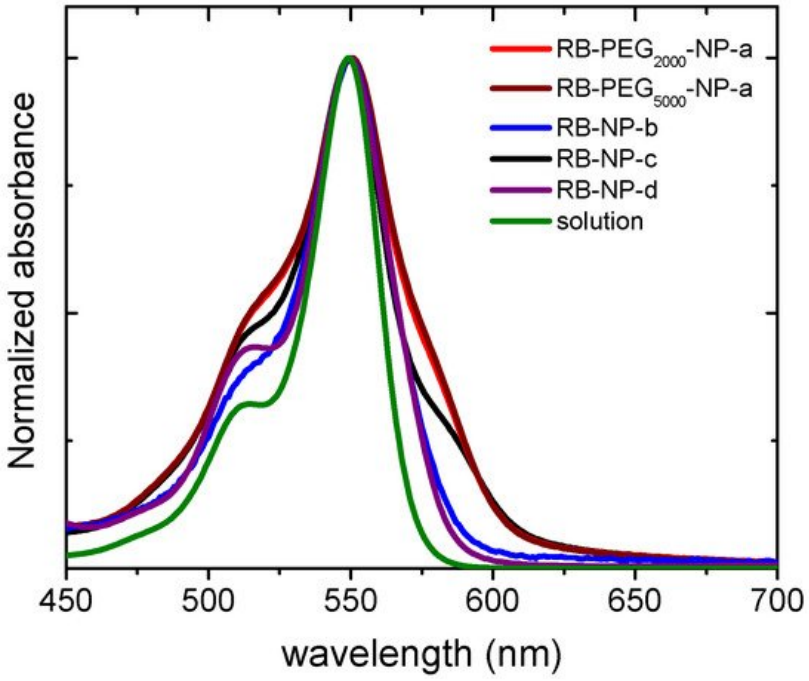

Figure 3. Normalized absorption spectra of RB-PEG_{2000}-NP-**a** (**red**), RB-PEG_{5000}-NP-**a** (**brown**), RB-PEG-NP-**b** (**blue**), RB-PEG-NP-**c** (**black**), RB-PEG-NP-**d** (**purple**) in water suspension (0.5 mg/mL) and RB in diluted aqueous solution (**green**). The absorption spectra were recorded after stirring the nanosystems for at least 24 h.

References

1. Dolmans, D.E.J.G.J.; Fukumura, D.; Jain, R.K. Photodynamic therapy for cancer. Nat. Rev. Cancer 2003, 3, 380–387.
2. Dąbrowski, J.M.; Arnaut, L.G. Photodynamic therapy (PDT) of cancer: From local to systemic treatment. Photochem. Photobiol. Sci. 2015, 14, 1765–1780.
3. Hopper, C. Photodynamic therapy: A clinical reality in the treatment of cancer. Lancet Oncol. 2000, 1, 212–219.
4. Moghissi, K.; Dixon, K.; Gibbins, S. A Surgical View of Photodynamic Therapy in Oncology: A Review. Surg. J. 2015, 1, e1–e15.
5. Lin, J.; Wan, M.T. Current evidence and applications of photodynamic therapy in dermatology. Clin. Cosmet. Investig. Dermatol. 2014, 7, 145.
6. DeRosa, M. Photosensitized singlet oxygen and its applications. Coord. Chem. Rev. 2002, 233–234, 351–371.
7. Nonell, S.; Flors, C. (Eds.) Singlet Oxygen, Applications in Biosciences and Nanosciences; Royal Society of Chemistry: Cambridge, UK, 2016; ISBN 978-1-78262-038-9.
8. Huang, Z. A review of progress in clinical photodynamic therapy. Technol. Cancer Res. Treat. 2005, 4, 283–293.
9. Stallivieri, A.; Colombeau, L.; Jetpisbayeva, G.; Moussaron, A.; Myrzakhmetov, B.; Arnoux, P.; Acherar, S.; Vanderesse, R.; Frochot, C. Folic acid conjugates with photosensitizers for cancer targeting in photodynamic therapy: Synthesis and photophysical properties. Bioorg. Med. Chem. 2017, 25, 1–10.
10. Lacombe, S.; Pigot, T. Materials for selective photo-oxygenation vs. photocatalysis: Preparation, properties and applications in environmental and health fields. Catal. Sci. Technol. 2016, 6, 1571–1592.
11. Lucky, S.S.; Soo, K.C.; Zhang, Y. Nanoparticles in Photodynamic Therapy. Chem. Rev. 2015, 115, 1990–2042.
12. Yin, R.; Hamblin, M. Antimicrobial Photosensitizers: Drug Discovery Under the Spotlight. Curr. Med. Chem. 2015, 22, 2159–2185.
13. Li, X.; Kolemen, S.; Yoon, J.; Akkaya, E.U. Activatable Photosensitizers: Agents for Selective Photodynamic Therapy. Adv. Funct. Mater. 2017, 27, 1604053.
14. Blázquez-Moraleja, A.; Álvarez-Fernández, D.; Prieto Montero, R.; García-Moreno, I.; Martínez-Martínez, V.; Bañuelos, J.; Sáenz-de-Santa-María, I.; Chiara, M.D.; Chiara, J.L. A general modular approach for the solubility tagging of

BODIPY dyes. Dye. Pigment. 2019, 170, 107545.

15. Zhang, X.F.; Yang, X. Photosensitizer that selectively generates singlet oxygen in nonpolar environments: Photophysical mechanism and efficiency for a covalent BODIPY dimer. J. Phys. Chem. B 2013, 117, 9050–9055.
16. Guan, Q.; Zhou, L.; Li, Y.; Dong, Y. Diiodo-Bodipy-Encapsulated Nanoscale Metal–Organic Framework for pH-Driven Selective and Mitochondria Targeted Photodynamic Therapy. Inorg. Chem. 2018, 57, 10137–10145.
17. Sánchez-Arroyo, A.J.; Palao, E.; Agarrabeitia, A.R.; Ortiz, M.J.; García-Fresnadillo, D. Towards improved halogenated BODIPY photosensitizers: Clues on structural designs and heavy atom substitution patterns. Phys. Chem. Chem. Phys. 2017, 19, 69–72.
18. Prieto-Montero, R.; Prieto-Castañeda, A.; Sola-Llano, R.; Agarrabeitia, A.R.; García-Fresnadillo, D.; López-Arbeloa, I.; Villanueva, A.; Ortiz, M.J.; Moya, S.; Martínez-Martínez, V. Exploring BODIPY Derivatives as Singlet Oxygen Photosensitizers for PDT. Photochem. Photobiol. 2020, 96, 458–477.
19. López Arbeloa, F.; Bañuelos, J.; Martínez, V.; Arbeloa, T.; López Arbeloa, I. Structural, photophysical and lasing properties of pyrromethene dyes. Int. Rev. Phys. Chem. 2005, 24, 339–374.
20. Prieto, J.B.; Arbeloa, F.L.; Martínez, V.M.; López, T.A.; Arbeloa, I.L. Photophysical properties of the pyrromethene 597 dye: Solvent effect. J. Phys. Chem. A 2004, 108, 5503–5508.
21. Wang, D.G.; Zhang, L.N.; Li, Q.; Yang, Y.; Wu, Y.; Fan, X.; Song, M.; Kuang, G.C. Dimeric BODIPYs with different linkages: A systematic investigation on structure-properties relationship. Tetrahedron 2017, 73, 6894–6900.
22. Esnal, I.; Valois-Escamilla, I.; Gõmez-Durán, C.F.; Urías-Benavides, A.; Betancourt-Mendiola, M.L.; Lõpez-Arbeloa, I.; Bañuelos, J.; García-Moreno, I.; Costela, A.; Peña-Cabrera, E. Blue-to-orange color-tunable laser emission from tailored boron-dipyrromethene dyes. ChemPhysChem 2013, 14, 4134–4142.
23. Epelde-Elezcano, N.; Martínez-Martínez, V.; Peña-Cabrera, E.; Gómez-Durán, C.F.A.; López-Arbeloa, I.; Lacombe, S. Modulation of singlet oxygen generation in halogenated BODIPY dyes by substitution at their meso position: Towards a solvent-independent standard in the vis region. RSC Adv. 2016, 6, 41991–41998.
24. Loudet, A.; Burgess, K. BODIPY dyes and their derivatives: Syntheses and spectroscopic properties. Chem. Rev. 2007, 107, 4891–4932.
25. Bañuelos, J. BODIPY Dye, the Most Versatile Fluorophore Ever? Chem. Rec. 2016, 16, 335–348.
26. Kamkaew, A.; Lim, S.H.; Lee, H.B.; Kiew, L.V.; Chung, L.Y.; Burgess, K. BODIPY dyes in photodynamic therapy. Chem. Soc. Rev. 2013, 42, 77–88.
27. Palao-Utiel, E.; Montalvillo-Jiménez, L.; Esnal, I.; Prieto-Montero, R.; Agarrabeitia, A.R.; García-Moreno, I.; Bañuelos, J.; López-Arbeloa, I.; de la Moya, S.; Ortiz, M.J. Controlling Vilsmeier-Haack processes in meso-methylBODIPYs: A new way to modulate finely photophysical properties in boron dipyrromethenes. Dye. Pigment. 2017, 141, 286–298.
28. Turksoy, A.; Yildiz, D.; Akkaya, E.U. Photosensitization and controlled photosensitization with BODIPY dyes. Coord. Chem. Rev. 2019, 379, 47–64.
29. Zhang, X.F.; Feng, N. Photoinduced Electron Transfer-based Halogen-free Photosensitizers: Covalent meso-Aryl (Phenyl, Naphthyl, Anthryl, and Pyrenyl) as Electron Donors to Effectively Induce the Formation of the Excited Triplet State and Singlet Oxygen for BODIPY Compounds. Chem. An Asian J. 2017, 2447–2456.
30. Jiménez, J.; Prieto-Montero, R.; Maroto, B.L.; Moreno, F.; Ortiz, M.J.; Oliden-Sánchez, A.; López-Arbeloa, I.; Martínez-Martínez, V.; de la Moya, S. Manipulating Charge-Transfer States in BODIPYs: A Model Strategy to Rapidly Develop Photodynamic Theragnostic Agents. Chem. A Eur. J. 2020, 26, 601–605.
31. Kim, B.; Sui, B.; Yue, X.; Tang, S.; Tichy, M.G.; Belfield, K.D. In Vitro Photodynamic Studies of a BODIPY-Based Photosensitizer. European J. Org. Chem. 2017, 2017, 25–28.
32. Ziessel, R.; Ulrich, G.; Haefele, A.; Harriman, A. An artificial light-harvesting array constructed from multiple bodipy dyes. J. Am. Chem. Soc. 2013, 135, 11330–11344.
33. Gorbe, M.; Costero, A.M.; Sancenón, F.; Martínez-Máñez, R.; Ballesteros-Cillero, R.; Ochando, L.E.; Chulvi, K.; Gotor, R.; Gil, S. Halogen-containing BODIPY derivatives for photodynamic therapy. Dye. Pigment. 2019, 160, 198–207.
34. Atilgan, S.; Ekmekci, Z.; Dogan, A.L.; Guc, D.; Akkaya, E.U. Water soluble distyryl-boradiazaindacenes as efficient photosensitizers for photodynamic therapy. Chem. Commun. 2006, 4398–4400.
35. Ke, M.R.; Yeung, S.L.; Ng, D.K.P.; Fong, W.P.; Lo, P.C. Preparation and in vitro photodynamic activities of folate-conjugated distyryl boron dipyrromethene based photosensitizers. J. Med. Chem. 2013, 56, 8475–8483.
36. Xiong, H.; Zhou, K.; Yan, Y.; Miller, J.B.; Siegwart, D.J. Tumor-Activated Water-Soluble Photosensitizers for Near-Infrared Photodynamic Cancer Therapy. ACS Appl. Mater. Interfaces 2018, 10, 16335–16343.

37. He, H.; Lo, P.C.; Yeung, S.L.; Fong, W.P.; Ng, D.K.P. Synthesis and in vitro photodynamic activities of pegylated distyryl boron dipyrromethene derivatives. J. Med. Chem. 2011, 54, 3097–3102.

38. Simões, J.C.S.; Sarpaki, S.; Papadimitroulas, P.; Therrien, B.; Loudos, G. Conjugated Photosensitizers for Imaging and PDT in Cancer Research. J. Med. Chem. 2020, 63, 14119–14150.

39. Khuong Mai, D.; Kang, B.; Pegarro Vales, T.; Badon, I.W.; Cho, S.; Lee, J.; Kim, E.; Kim, H.-J. Synthesis and Photophysical Properties of Tumor-Targeted Water-Soluble BODIPY Photosensitizers for Photodynamic Therapy. Molecules 2020, 25, 3340.

40. Chaturvedi, V.K.; Singh, A.; Singh, V.K.; Singh, M.P. Cancer Nanotechnology: A New Revolution for Cancer Diagnosis and Therapy. Curr. Drug Metab. 2018, 20, 416–429.

41. Mirabello, V.; Calatayud, D.G.; Arrowsmith, R.L.; Ge, H.; Pascu, S.I. Metallic nanoparticles as synthetic building blocks for cancer diagnostics: From materials design to molecular imaging applications. J. Mater. Chem. B 2015, 3, 5657–5672.

42. Bobo, D.; Robinson, K.J.; Islam, J.; Thurecht, K.J.; Corrie, S.R. Nanoparticle-Based Medicines: A Review of FDA-Approved Materials and Clinical Trials to Date. Pharm. Res. 2016, 33, 2373–2387.

43. Zhuang, Y.; Zhao, L.; Zheng, L.; Hu, Y.; Ding, L.; Li, X.; Liu, C.; Zhao, J.; Shi, X.; Guo, R. LAPONITE-Polyethylenimine Based Theranostic Nanoplatform for Tumor-Targeting CT Imaging and Chemotherapy. ACS Biomater. Sci. Eng. 2017, 3, 431–442.

44. Alexis, F.; Pridgen, E.; Molnar, L.K.; Farokhzad, O.C. Factors affecting the clearance and biodistribution of polymeric nanoparticles. Mol. Pharm. 2008, 5, 505–515.

45. Mousa, M.; Evans, N.D.; Oreffo, R.O.C.; Dawson, J.I. Clay nanoparticles for regenerative medicine and biomaterial design: A review of clay bioactivity. Biomaterials 2018, 159, 204–214.

46. Rudramurthy, G.R.; Swamy, M.K. Potential applications of engineered nanoparticles in medicine and biology: An update. JBIC J. Biol. Inorg. Chem. 2018, 23, 1185–1204.

47. Conde, J.; Dias, J.T.; Grazú, V.; Moros, M.; Baptista, P.V.; de la Fuente, J.M. Revisiting 30 years of biofunctionalization and surface chemistry of inorganic nanoparticles for nanomedicine. Front. Chem. 2014, 2.

48. Adumeau, L.; Genevois, C.; Roudier, L.; Schatz, C.; Couillaud, F.; Mornet, S. Impact of surface grafting density of PEG macromolecules on dually fluorescent silica nanoparticles used for the in vivo imaging of subcutaneous tumors. Biochim. Biophys. Acta Gen. Subj. 2017, 1861, 1587–1596.

49. Dawidczyk, C.M.; Kim, C.; Park, J.H.; Russell, L.M.; Lee, K.H.; Pomper, M.G.; Searson, P.C. State-of-the-art in design rules for drug delivery platforms: Lessons learned from FDA-approved nanomedicines. J. Control. Release 2014, 187, 133–144.

50. Son, J.; Yang, S.M.; Yi, G.; Roh, Y.J.; Park, H.; Park, J.M.; Choi, M.; Koo, H. Folate-modified PLGA nanoparticles for tumor-targeted delivery of pheophorbide a in vivo. Biochem. Biophys. Res. Commun. 2018, 498, 523–528.

51. Zhang, Q.; Liu, F.; Nguyen, K.T.; Ma, X.; Wang, X.; Xing, B.; Zhao, Y. Multifunctional Mesoporous Silica Nanoparticles for Cancer-Targeted and Controlled Drug Delivery. Adv. Funct. Mater. 2012, 22, 5144–5156.

52. Villaverde, G.; Baeza, A.; Melen, G.J.; Alfranca, A.; Ramirez, M.; Vallet-Regí, M. A new targeting agent for the selective drug delivery of nanocarriers for treating neuroblastoma. J. Mater. Chem. B 2015, 3, 4831–4842.

53. Ribeiro, T.; Prazeres, T.J.V.; Moffitt, M.; Farinha, J.P.S. Enhanced Photoluminescence from Micellar Assemblies of Cadmium Sulfide Quantum Dots and Gold Nanoparticles. J. Phys. Chem. C 2013, 117, 3122–3133.

54. Pérez, N.; Ruiz-Rubio, L.; Vilas, J.L.; Rodríguez, M.; Martinez-Martinez, V.; León, L.M. Synthesis and characterization of near-infrared fluorescent and magnetic iron zero-valent nanoparticles. J. Photochem. Photobiol. A Chem. 2016, 315, 1–7.

55. Jeevanandam, J.; Barhoum, A.; Chan, Y.S.; Dufresne, A.; Danquah, M.K. Review on nanoparticles and nanostructured materials: History, sources, toxicity and regulations. Beilstein J. Nanotechnol. 2018, 9, 1050–1074.

56. Malvindi, M.A.; Brunetti, V.; Vecchio, G.; Galeone, A.; Cingolani, R.; Pompa, P.P. SiO2 nanoparticles biocompatibility and their potential for gene delivery and silencing. Nanoscale 2012, 4, 486–495.

57. Wheeler, P.A.; Wang, J.; Baker, J.; Mathias, L.J. Synthesis and characterization of covalently functionalized laponite clay. Chem. Mater. 2005, 17, 3012–3018.

58. Kuang, G.; Zhang, Q.; He, S.; Liu, Y. Curcumin-loaded PEGylated mesoporous silica nanoparticles for effective photodynamic therapy. RSC Adv. 2020, 10, 24624–24630.

59. Chen, K.; Chang, C.; Liu, Z.; Zhou, Y.; Xu, Q.; Li, C.; Huang, Z.; Xu, H.; Xu, P.; Lu, B. Hyaluronic acid targeted and pH-responsive nanocarriers based on hollow mesoporous silica nanoparticles for chemo-photodynamic combination

therapy. Colloids Surf. B Biointerfaces 2020, 194.

60. Lyles, Z.K.; Tarannum, M.; Mena, C.; Inada, N.M.; Bagnato, V.S.; Vivero-Escoto, J.L. Biodegradable Silica-Based Nanoparticles with Improved and Safe Delivery of Protoporphyrin IX for the In Vivo Photodynamic Therapy of Breast Cancer. Adv. Ther. 2020, 3, 2000022.
61. Ellahioui, Y.; Patra, M.; Mari, C.; Kaabi, R.; Karges, J.; Gasser, G.; Gómez-Ruiz, S. Mesoporous silica nanoparticles functionalised with a photoactive ruthenium(ii) complex: Exploring the formulation of a metal-based photodynamic therapy photosensitiser. Dalt. Trans. 2019, 48, 5940–5951.
62. Figueira, F.; Cavaleiro, J.A.S.; Tomé, J.P.C. Silica nanoparticles functionalized with porphyrins and analogs for biomedical studies. J. Porphyr. Phthalocyanines 2011, 15, 517–533.
63. Martins Estevão, B.; Miletto, I.; Marchese, L.; Gianotti, E. Optimized Rhodamine B labeled mesoporous silica nanoparticles as fluorescent scaffolds for the immobilization of photosensitizers: A theranostic platform for optical imaging and photodynamic therapy. Phys. Chem. Chem. Phys. 2016, 18, 9042–9052.
64. Ronzani, F.; Costarramone, N.; Blanc, S.; Benabbou, A.K.; Le Bechec, M.; Pigot, T.; Oelgemöller, M.; Lacombe, S. Visible-light photosensitized oxidation of α-terpinene using novel silica-supported sensitizers: Photooxygenation vs. photodehydrogenation. J. Catal. 2013, 303, 164–174.
65. Gianotti, E.; Martins Estevão, B.; Cucinotta, F.; Hioka, N.; Rizzi, M.; Renò, F.; Marchese, L. An Efficient Rose Bengal Based Nanoplatform for Photodynamic Therapy. Chem. A Eur. J. 2014, 20, 10921–10925.
66. Cheng, S.-H.; Lee, C.-H.; Yang, C.-S.; Tseng, F.-G.; Mou, C.-Y.; Lo, L. Mesoporous silica nanoparticles functionalized with an oxygen-sensing probe for cell photodynamic therapy: Potential cancer theranostics. J. Mater. Chem. 2009, 19, 1252.
67. Martins Estevão, B.; Cucinotta, F.; Hioka, N.; Cossi, M.; Argeri, M.; Paul, G.; Marchese, L.; Gianotti, E. Rose Bengal incorporated in mesostructured silica nanoparticles: Structural characterization, theoretical modeling and singlet oxygen delivery. Phys. Chem. Chem. Phys. 2015, 17, 26804–26812.
68. Kan, J.L.; Jiang, Y.; Xue, A.; Yu, Y.H.; Wang, Q.; Zhou, Y.; Dong, Y. Bin Surface Decorated Porphyrinic Nanoscale Metal-Organic Framework for Photodynamic Therapy. Inorg. Chem. 2018, 57, 5420–5428.
69. Wang, S.; Fan, W.; Kim, G.; Hah, H.J.; Lee, Y.E.K.; Kopelman, R.; Ethirajan, M.; Gupta, A.; Goswami, L.N.; Pera, P.; et al. Novel methods to incorporate photosensitizers into nanocarriers for cancer treatment by photodynamic therapy. Lasers Surg. Med. 2011, 43, 686–695.
70. Tada, D.B.; Baptista, M.S. Photosensitizing nanoparticles and the modulation of ROS generation. Front. Chem. 2015, 3, 1–14.
71. Hu, W.; Ma, H.; Hou, B.; Zhao, H.; Ji, Y.; Jiang, R.; Hu, X.; Lu, X.; Zhang, L.; Tang, Y.; et al. Engineering Lysosome-Targeting BODIPY Nanoparticles for Photoacoustic Imaging and Photodynamic Therapy under Near-Infrared Light. ACS Appl. Mater. Interfaces 2016, 8, 12039–12047.
72. Liu, N.; Zhu, M.; Niu, N.; Ren, J.; Yang, N.; Yu, C. Aza-BODIPY Probe-Decorated Mesoporous Black TiO2Nanoplatform for the Highly Efficient Synergistic Phototherapy. ACS Appl. Mater. Interfaces 2020, 12, 41071–41078.
73. Mangalath, S.; Saneesh Babu, P.S.; Nair, R.R.; Manu, P.M.; Krishna, S.; Nair, S.A.; Joseph, J. Graphene Quantum Dots Decorated with Boron Dipyrromethene Dye Derivatives for Photodynamic Therapy. ACS Appl. Nano Mater. 2021, 4, 4162–4171.
74. Chen, J.; Cui, Y.; Song, K.; Liu, T.; Zhou, L.; Bao, B.; Wang, R.; Wang, L. The self-assembly of a hybrid photosensitizer for the synergistically enhanced photodynamic/photothermal therapy. Biomater. Sci. 2021, 9, 2115–2123.
75. Li, R.; Du, Y.; Guo, W.; Su, Y.; Meng, Y.; Shan, Z.; Feng, Y.; Meng, S. Methotrexate coated AZA-BODIPY nanoparticles for chemotherapy, photothermal and photodynamic synergistic therapy. Dye. Pigment. 2020, 179, 108351.
76. Bartelmess, J.; Milcovich, G.; Maffeis, V.; d'Amora, M.; Bertozzi, S.M.; Giordani, S. Modulation of Efficient Diiodo-BODIPY in vitro Phototoxicity to Cancer Cells by Carbon Nano-Onions. Front. Chem. 2020, 8, 1–9.
77. González-Béjar, M.; Liras, M.; Francés-Soriano, L.; Voliani, V.; Herranz-Pérez, V.; Duran-Moreno, M.; Garcia-Verdugo, J.M.; Alarcon, E.I.; Scaiano, J.C.; Pérez-Prieto, J. NIR excitation of upconversion nanohybrids containing a surface grafted Bodipy induces oxygen-mediated cancer cell death. J. Mater. Chem. B 2014, 2, 4554.
78. Chauhan, P.; Yan, N. Novel bodipy—Cellulose nanohybrids for the production of singlet oxygen. RSC Adv. 2016, 6, 32070–32073.
79. Ruan, Z.; Liu, L.; Jiang, W.; Li, S.; Wang, Y.; Yan, L. NIR imaging-guided combined photodynamic therapy and chemotherapy by a pH-responsive amphiphilic polypeptide prodrug. Biomater. Sci. 2017, 5, 313–321.

80. Sun, W.; Zhao, X.; Fan, J.; Du, J.; Peng, X. Boron Dipyrromethene Nano-Photosensitizers for Anticancer Phototherapies. Small 2019, 1804927, 1–25.

81. Chen, X.-Z.; Hoop, M.; Shamsudhin, N.; Huang, T.; Özkale, B.; Li, Q.; Siringil, E.; Mushtaq, F.; Di Tizio, L.; Nelson, B.J.; et al. Hybrid Magnetoelectric Nanowires for Nanorobotic Applications: Fabrication, Magnetoelectric Coupling, and Magnetically Assisted In Vitro Targeted Drug Delivery. Adv. Mater. 2017, 29, 1605458–1605465.

82. Zhang, Q.; Cai, Y.; Wang, X.J.; Xu, J.L.; Ye, Z.; Wang, S.; Seeberger, P.H.; Yin, J. Targeted Photodynamic Killing of Breast Cancer Cells Employing Heptamannosylated β-Cyclodextrin-Mediated Nanoparticle Formation of an Adamantane-Functionalized BODIPY Photosensitizer. ACS Appl. Mater. Interfaces 2016, 8, 33405–33411.

83. Zong, J.; Peng, H.; Qing, X.; Fan, Z.; Xu, W.; Du, X.; Shi, R.; Zhang, Y. pH-Responsive Pluronic F127–Lenvatinib-Encapsulated Halogenated Boron-Dipyrromethene Nanoparticles for Combined Photodynamic Therapy and Chemotherapy of Liver Cancer. ACS Omega 2021, 6, 12331–12342.

84. Deng, J.; Yang, M.; Li, C.; Liu, G.; Sun, Q.; Luo, X.; Wu, F. Single molecular-based nanoparticles with aggregation-induced emission characteristics for fluorescence imaging and efficient cancer phototherapy. Dye. Pigment. 2021, 187, 109130.

85. Das, A.; Shome, A.; Manna, U. Porous and reactive polymeric interfaces: An emerging avenue for achieving durable and functional bio-inspired wettability. J. Mater. Chem. A 2021, 9, 824–856.

86. Li, M.; Li, X.; Cao, Z.; Wu, Y.; Chen, J.A.; Gao, J.; Wang, Z.; Guo, W.; Gu, X. Mitochondria-targeting BODIPY-loaded micelles as novel class of photosensitizer for photodynamic therapy. Eur. J. Med. Chem. 2018, 157, 599–609.

87. Chang, Z.; Ye, J.H.; Qi, F.; Fang, H.; Lin, F.; Wang, S.; Mu, C.; Zhang, W.; He, W. A PEGylated photosensitizer-core pH-responsive polymeric nanocarrier for imaging-guided combination chemotherapy and photodynamic therapy. New J. Chem. 2021, 45, 6180–6185.

88. Perumal, D.; Golla, M.; Pillai, K.S.; Raj, G.; Anusree Krishna, P.K.; Varghese, R. Biotin-decorated NIR-absorbing nanosheets for targeted photodynamic cancer therapy. Org. Biomol. Chem. 2021, 19, 2804–2810.

89. Wang, Z.; Hong, X.; Zong, S.; Tang, C.; Cui, Y.; Zheng, Q. BODIPY-doped silica nanoparticles with reduced dye leakage and enhanced singlet oxygen generation. Sci. Rep. 2015, 5, 12602.

90. Zhu, Y.; Song, N.; Chen, L.; Xie, Z. Reduction responsive BODIPY decorated mesoporous silica nanoscale platforms for photodynamic therapy. Microporous Mesoporous Mater. 2021, 311, 110689.

91. Alexander, W. American society of clinical oncology, 2010 annual meeting and Rose Bengal: From a wool dye to a cancer therapy. Pharm. Ther. 2010, 35, 469–478.

92. Gualdesi, M.S.; Vara, J.; Aiassa, V.; Alvarez Igarzabal, C.I.; Ortiz, C.S. Thionine in the design of new photosensitizers: Bromination and vehiculization in polymeric nanoparticles. J. Mol. Liq. 2020, 310, 113247.

93. Tuite, E.M.; Kelly, J.M. New trends in photobiology. Photochemical interactions of methylene blue and analogues with DNA and other biological substrates. J. Photochem. Photobiol. B Biol. 1993, 21, 103–124.

94. Zahraei, M.; Marciello, M.; Lazaro-Carrillo, A.; Villanueva, A.; Herranz, F.; Talelli, M.; Costo, R.; Monshi, A.; Shahbazi-Gahrouei, D.; Amirnasr, M.; et al. Versatile theranostics agents designed by coating ferrite nanoparticles with biocompatible polymers. Nanotechnology 2016, 27, 255702.

95. Asefa, T.; Tao, Z. Biocompatibility of mesoporous silica nanoparticles. Chem. Res. Toxicol. 2012, 25, 2265–2284.

96. He, Q.; Zhang, J.; Shi, J.; Zhu, Z.; Zhang, L.; Bu, W.; Guo, L.; Chen, Y. The effect of PEGylation of mesoporous silica nanoparticles on nonspecific binding of serum proteins and cellular responses. Biomaterials 2010, 31, 1085–1092.

97. Suk, J.S.; Xu, Q.; Kim, N.; Hanes, J.; Ensign, L.M. PEGylation as a strategy for improving nanoparticle-based drug and gene delivery. Adv. Drug Deliv. Rev. 2016, 99, 28–51.

98. Manzano, M.; Vallet-Regí, M. Mesoporous Silica Nanoparticles for Drug Delivery. Adv. Funct. Mater. 2020, 30, 1902634.

99. Mai, W.X.; Meng, H. Mesoporous silica nanoparticles: A multifunctional nano therapeutic system. Integr. Biol. 2013, 5, 19–28.

100. Stöber, W.; Fink, A.; Bohn, E. Controlled growth of monodisperse silica spheres in the micron size range. J. Colloid Interface Sci. 1968, 26, 62–69.

101. Prieto-Montero, R.; Katsumiti, A.; Cajaraville, M.P.; Lopez Arbeloa, I.; Martinez-Martinez, V. Functionalized Fluorescent Silica Nanoparticles for Bioimaging of Cancer Cells. Sensors 2020, 20, 5590.

102. Arulprakasajothi, M.; Elangovan, K.; Chandrasekhar, U.; Suresh, S. Performance Study of Conical Strip Inserts in Tube Heat. Therm. Sci. 2018, 22, 477–485.

103. Epelde-Elezcano, N.; Prieto-Montero, R.; Martínez-Martínez, V.; Ortiz, M.J.; Prieto-Castañeda, A.; Peña-Cabrera, E.; Belmonte-Vázquez, J.L.; López-Arbeloa, I.; Brown, R.; Lacombe, S. Adapting BODIPYs to singlet oxygen production on silica nanoparticles. Phys. Chem. Chem. Phys. 2017, 19, 13746–13755.
104. Maurel, M.; Montheil, T.; Martin, J.; Chaar, L.; Guzman-Gonzalez, V.; Couvet, M.; Jacquet, T.; Jia, T.; Eymin, B.; Parra, K.; et al. Design of pegylated three ligands silica nanoparticles for multi-receptor targeting. Nanomaterials 2021, 11, 177.
105. Cruz, L.J.; Tacken, P.J.; Fokkink, R.; Figdor, C.G. The influence of PEG chain length and targeting moiety on antibody-mediated delivery of nanoparticle vaccines to human dendritic cells. Biomaterials 2011, 32, 6791–6803.
106. Chithrani, D.B. Polyethylene Glycol Density and Length Affects Nanoparticle Uptake by Cancer Cells. J. Nanomed. Res. 2014, 1, 1–6.